Nanoscale Res Lett (2010) 5:1344–1350
DOI 10.1007/s11671-010-9651-9

NANO EXPRESS

Glassy State Lead Tellurite Nanobelts: Synthesis and Properties

Buyong Wan · Chenguo Hu · Hong Liu · Xueyan Chen · Yi Xi · Xiaoshan He

Received: 30 March 2010 / Accepted: 17 May 2010 / Published online: 4 June 2010

Abstract The lead tellurite nanobelts have been first synthesized in the composite molten salts (KNO_3/$LiNO_3$) method, which is cost-effective, one-step, easy to control, and performed at low-temperature and in ambient atmosphere. Scanning electron microscopy, X-ray diffraction, transmission electron microscopy, X-ray photoelectron spectrum, energy dispersive X-ray spectroscopy and FT-IR spectrum are used to characterize the structure, morphology, and composition of the samples. The results show that the as-synthesized products are amorphous and glassy nanobelts with widths of 200–300 nm and lengths up to tens of microns and the atomic ratio of Pb:Te:O is close to 1:1.5:4. Thermo-gravimetric analysis (TGA) and differential scanning calorimetry (DSC) and investigations of the corresponding structure and morphology change confirm that the nanobelts have low glass transition temperature and thermal stability. Optical diffuse reflectance spectrum indicates that the lead tellurite nanobelts have two optical gaps at ca. 3.72 eV and 4.12 eV. Photoluminescence (PL) spectrum and fluorescence imaging of the products exhibit a blue emission (round 480 nm).

B. Wan · C. Hu (✉) · Y. Xi · X. He
Department of Applied Physics, Chongqing University, 400044 Chongqing, People's Republic of China
e-mail: hucg@cqu.edu.cn

B. Wan
Key Laboratory of Optical Engineering, College of Physics and Information Technology, Chongqing Normal University, 400047 Chongqing, People's Republic of China

H. Liu · X. Chen
State Key Laboratory of Crystal Materials, Shandong University, 250100 Jinan, People's Republic of China

Keywords Chemical synthesis · Lead tellurite · Nanostructures · Molten salt · Photoluminescence

Introduction

Tellurite glasses are of great interest because of their interesting electrical and optical properties such as high refractive index, low phonon energy, wide transmission window in the infrared range, and nonlinear optical behaviors, etc. [1, 2]. The heavy metals oxides or other oxides with empty *d* orbital, such PbO, Bi_2O_3, and Nb_2O_5, have been incorporated for enhancing the optical behavior of tellurite glasses, which have application in all-optical switching, optical limiters, IR domes, laser windows, and other optical devices [1–6]. Especially, rare earth ion such as Er^{3+}, Yb^{3+} activated tellurite glasses exhibit the outstanding properties in energy transfer, upconversion luminescence and optical communications [7–12].

The tellurite glasses are prepared with conventional melting procedures, which involve powder fusion over 1,000 K and quenching melts at hundreds of Kelvins. Commonly, the products are bulky and their micro-structures have been rarely characterized. It was reported [13, 14] that the tellurite glass fibers have application in infrared and nonlinear optics. When the dimension of the tellurite glass decreases and even to one-dimension, how are their properties? Nowadays, nanomaterials (including nanowire [15, 16], nanotubes [17, 18], nanobelts [19, 20], et al.) have attracted much attention due to their outstanding physical and chemical properties. However, up to now, few tellurite nano-materials and their properties have been reported.

Herein, we have developed an approach for synthesis of lead tellurite glassy nanobelts, which has the advantages of

one-step, easy scale-up, low cost and environmentally friendly. The thermal and optical properties of the lead tellurite nanobelts have been investigated for the first time.

Experimental

All chemicals were used as received without further purification. The synthesis of the lead tellurite nanobelts follows the steps: An amount of 18 g of mixed salts (KNO_3:$LiNO_3$ = 42.4:57.6) was placed in a 50-ml ceramic crucible and mixed uniformly, the crucible was put on a stirring hotplate, which was preheated to 210°C. After the salts were totally molten, a magnetic stirring bar was placed in it and let it stir at 800 r/min in ambient atmosphere, and then 1 mmol tellurium (Te) powder was added in the crucible. After the color of the melts fades slightly in about 1 h, 1 mmol lead nitrate $Pb(NO_3)_2$ was added into the melts and maintained there for 24 h. The crucible was then taken out and led cool naturally down to room-temperature. The solid product was dissolved in deionized water and then filtered. The collected product was washed by hot water and anhydrous ethanol.

The morphology and the size of the as-prepared samples were characterized by scanning electron microscopy at 20 kV (SEM, TESCAN VEGA2), and field emission scanning electron microscopy at 10 kV (FE-SEM, Nova 400 Nano SEM) and transmission electron microscopy at 400 kV (TEM, JEOL 4000EX). An energy dispersive X-ray spectroscopy (EDS) and X-ray diffractometer (XRD, BDX3200, China) with Cu Kα radiation (λ = 1.5418 Å) were used to investigate the crystal phase and chemical composition. The X-ray photoelectron spectra (XPS) were collected on an ESCALab MKII X-ray photoelectron spectrometer, using nonmonochromatized Mg Kα X-ray as the excitation source. Thermo-gravimetric analysis (TGA) and differential scanning calorimetry (DSC) for 5.10 mg of as-synthesized lead tellurite nanobelts were carried out under N_2 atmosphere at a heating rate of 10°C/min using a NETZSCH STA 449C simultaneous thermo-analyzer. An UV–Vis–NIR spectrophotometer (Hitachi U-4100) was used to measure the diffuse reflectance spectrum of the lead tellurite nanobelts. The FT-IR spectrum was obtained using KBr pellet on Thermo Nicolet FT-IR spectroscopy. The fluorescence imaging was carried out on an Olympus BX51 fluorescent microscope equipped with a 100 W mercury lamp. The room-temperature and low-temperature photoluminescence (PL) spectra were measured on the lead tellurite nanobelts on a glass slice under the irradiation of 30 mW HeCd laser at wavelength of 325 nm.

Results and Discussion

Morphologies of the Nanobelts

Typical SEM images of as-obtained lead tellurite nanobelts are shown in Fig. 1a, b. Figure 1a gives the low-magnified image of lead tellurite sample showing the nanowires with lengths up to tens of microns. Figure 1b gives the high-magnified image of the lead tellurite sample, in which the belt-like morphology can be seen with the width of 200–300 nm. EDS in Fig. 1c indicates that the elements in the product are Pb, Te, O, and Si, respectively (Si is from the substrate), and the atomic ratio of Pb, Te, and O is 1:1.58:6.40. Figure 1d shows the typical TEM image of a single nanobelt, which is consistent with the SEM observation in Fig. 1b. SAED pattern in Fig. 1e shows the diffuse amorphous diffraction ring, which indicates the nanobelts are of glassy state.

Formation Mechanism of Nanobelts

From the aforementioned experimental results, a possible reaction mechanism for the synthesis of the lead tellurite nanobelts in composite molten salts is suggested as the following. Although the melting points (T_m) of both pure potassium nitrate and lithium nitrate are over 250°C (T_m (KNO_3) = 337°C, T_m ($LiNO_3$) = 255°C), the eutectic point for the composition KNO_3/$LiNO_3$ = 42.4:57.6 is only about 130°C. In the melts, element Te powders are oxidized slowly under air atmosphere. As is well known, Te is a very important element as a glass former and can form tellurite-based glass with some metallic ions. Basic structure units of TeO_4 trigonal bipyramid (tbp), TeO_{3+1} polyhedra, TeO_3 trigonal pyramid (tp), and Te-eqOax-Te bond exist in TeO_2-based glasses [21], and the structural change of $[TeO_4] \rightarrow [TeO_{3+1}] \rightarrow [TeO_3]$ takes place along with the addition of modifier oxides. When PbO exists in the tellurite-based molten system, a large number of –O–Pb–O– linkages [22] with $[PbO_6]$ octahedra and $[OPb_4]$ and $[PbO_4]$ tetrahedra form and enter $[TeO_4]$ and $[TeO_3]$ network, and forms glass phase when the system cools down, because PbO can function as outside body or glass adjusting agent during the glass formation [23]. In this work, $Pb(NO_3)_2$ reacts with H_2O to produce $Pb(OH)_2$, and then form PbO polyhedra, which enter the Te–O-based network, and forms Pb–Te–O glass phase. Although both K and Na in the molten nitrate salt solution can function as glass adjusting agent, too, the large number of the ions makes them loss the chance to form glass with Te–O glass network. Compared with K and Na, a proper amount of PbO polyhedra is easily combined with Te–O network and forms glass during the cooling process. Besides, additional Pb oxide that enters into the glass matrix would create a

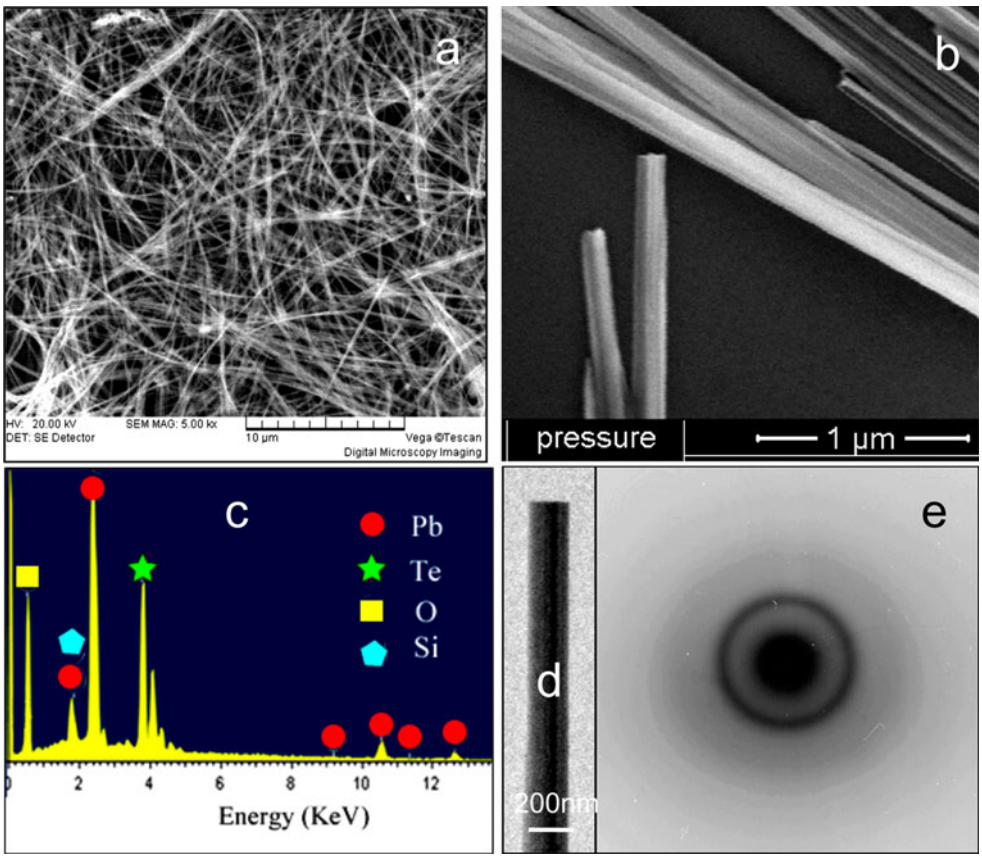

Fig. 1 SEM and TEM characterization of lead tellurite glassy nanobelts. **a** Low-magnification SEM images, indicating lengths of up to tens of microns, **b** high-magnification SEM images, indicating the belt-like shape of lead tellurite, **c** EDS spectra of lead tellurite, **d** is TEM image of a nanobelt and **e** the electron diffraction pattern

low rate of crystallization, since Pb oxide has the ability to form stable glass state due to its dual roles; one as glass former if Pb–O is covalent, the other as modifier if Pb–O is ionic [24, 25]. Under proper temperature and continuous stirring, the glass networks aggregate and then grow along certain direction to form belts. The whole process can be described diagrammatically in Scheme 1.

In particular, the continual stirring during the reaction and ambient atmosphere may be the key factors for the synthesis of lead tellurite nanobelts. Without stirring or intermittent stirring, a large number of unreacted elemental tellurium would be obtained, and no belt could be obtained. And, if the reactants were put in a sealed vessel, no belts were to be obtained, indicating the importance of existence of oxygen and water to the formation of lead tellurite nanobelts.

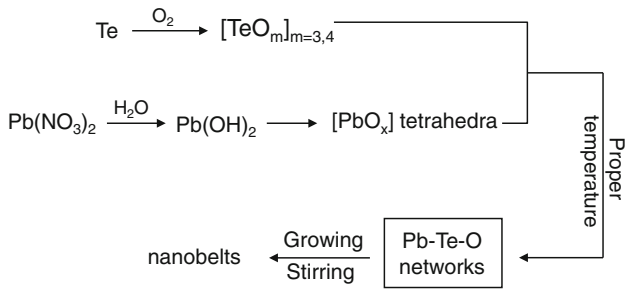

Scheme 1 Illustration of the formation process of lead tellurite nanobelts

The X-ray Photoelectron Spectra

XPS measurements were performed to further study the composition and oxidation states of Pb and Te in the lead tellurite nanobelts. The binding energies obtained in the XPS analysis were corrected for specimen charging by referencing the C 1s peak to 284.60 eV. The XPS spectrum of the lead tellurite in a wide energy range is shown in Fig. 2a. No obvious peaks for other elements or impurities besides carbon are observed. Figure 2b–d shows XPS taken from the Pb 4f, Te 3d, and O 1s regions of the nanobelts, respectively. The peak at a binding energy of 138.67 eV in Fig. 2b is primarily attributable to the Pb 4f 7/2 in lead tellurite, which is close to that of Pb ternary oxides such as $PbWO_4$ (138.7 eV) and $PbZrO_3$ (138.5 eV) [26]. The binding energy of Te 3d 5/2 at 576.61 eV in Fig. 2c is associated with TeO_3 [27]. In Fig. 2d, it can be seen that the O 1s profile is asymmetric, indicating that two oxygen species are present in the nearby region. The peak at ca. 530.24 eV can be indexed to the O (−2) in the lead tellurite, whereas the weaker shoulder peak at ca. 532.09 eV is due to chemisorbed oxygen caused by surface hydroxyl,

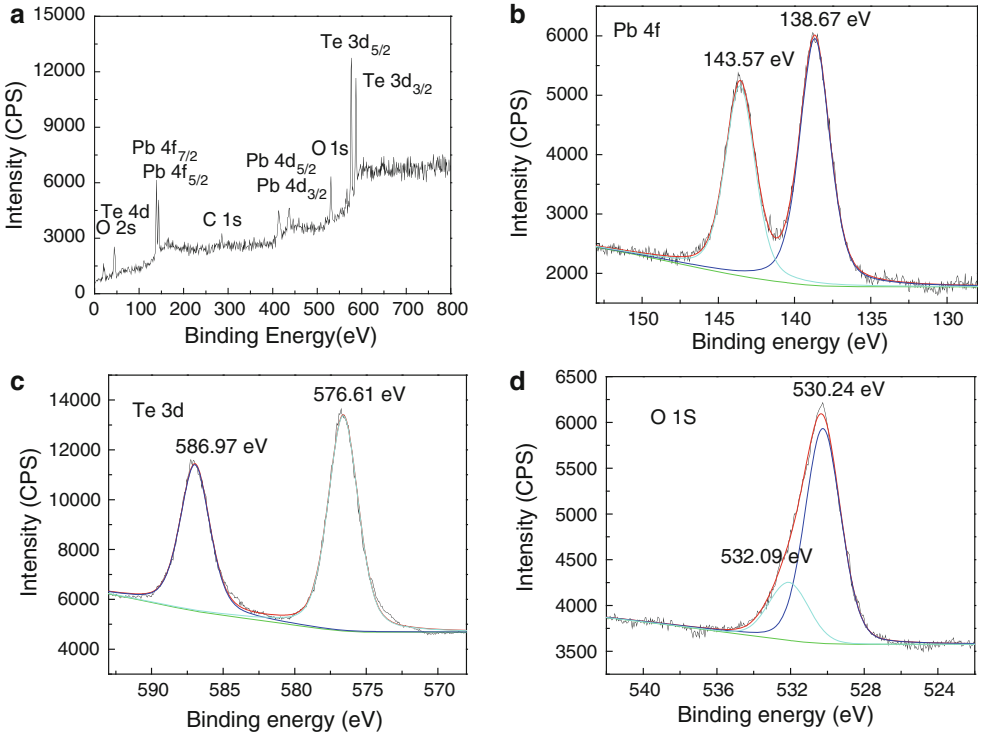

Fig. 2 High-resolution XPS spectra obtained in the lead tellurites. **a** Survey spectra, **b** Pb 4f spectra, **c** Te 3d spectra, **d** O 1s spectra

which corresponds to O–H bonds. The atomic composition of Pb, Te, and O is calculated using the integrated peak area and sensitivity factors, and atomic ratio of Pb:Te:O is 1:1.52:3.79. The ratio of Pb to Te is close to the result of EDS in Fig. 1c, but the oxygen content is less than that of EDS because the absorbing oxygen on the surface of the products has been disposed when Ar^+ ion bombardment clean the products before XPS test, while EDS test has no such procedure.

Temperature-Dependent State Transition

To obtain thermal properties of the lead tellurite, TGA and DSC experiments were carried out, and the results are shown in Fig. 3a. The increase in thermal treatment temperature is accompanied with the weight loss, and the overall observed weight loss (4.2% at 600°C) corresponds to the loss of the H_2O adsorbed on the surface of nanobelts and chemisorbed OH^- ions in the nanobelts, which occurs in approximately three steps. From the DSC data, the weight loss is simultaneously accompanied by endothermic and exothermic phenomena. For the tellurite glass, the glass transition temperature (T_g) gives information on both the strength of interatomic bonds and the glass network connectivity, in a similar way for the melting temperature for crystalline solids. In Fig. 3a, the onset of transition temperature (T_g) of lead tellurite glassy nanobelts is 261.61°C, and the peak of the crystallization temperature (T_c) is 292.71°C. The difference (ΔT) between T_c and T_g is only 31.1°C, far below that of bulky tellurite glasses [28–30], indicating the poor thermal stability of nanobelts. The low stability of the lead tellurite may be caused by its special structure of nanobelts that makes the glass network more relaxed. There are two strong endothermic peaks at 395.57 and 574.32°C, which may correspond to glass melting temperature (T_m). In order to understand information of the state transition of lead tellurite nanobelts, XRD spectra and SEM images are taken in accordance with DSC procedures at several intermediate temperatures: 250, 350, 500 and 600°C, respectively, which are shown in Fig. 3b–f. From Fig. 3b, after being annealed at 250°C, which is below the glass transition temperature (T_g), the nanobelts are still in amorphous state and their morphology have no change (Fig. 3c). At 350°C, which is over the crystallization temperature (T_c), some diffraction peaks begin to appear, which indicates that lead tellurite has crystallized. And deformation and distortion begin to occur in the belts, as is shown by the arrows in Fig. 3d. At 500°C, more diffractive peaks emerge, and the belts have shrunk and formed the pearl-necklace-shaped lead tellurite nanowires (Fig. 3e). At 600°C, the lead tellurite turns to the isolated micro-spheres, and the XRD pattern in Fig. 3b corresponds well to that of the literature data of $Pb_2Te_3O_8$ (JCPDS: 44-0568), which indicates that the products are of orthorhombic structure with lattice parameters of $a = 18.79$ Å, $b = 7.116$ Å and $c = 19.50$ Å. The stoichiometry of $Pb_2Te_3O_8$ is consistent with the results of the EDS and XPS before thermal treatment.

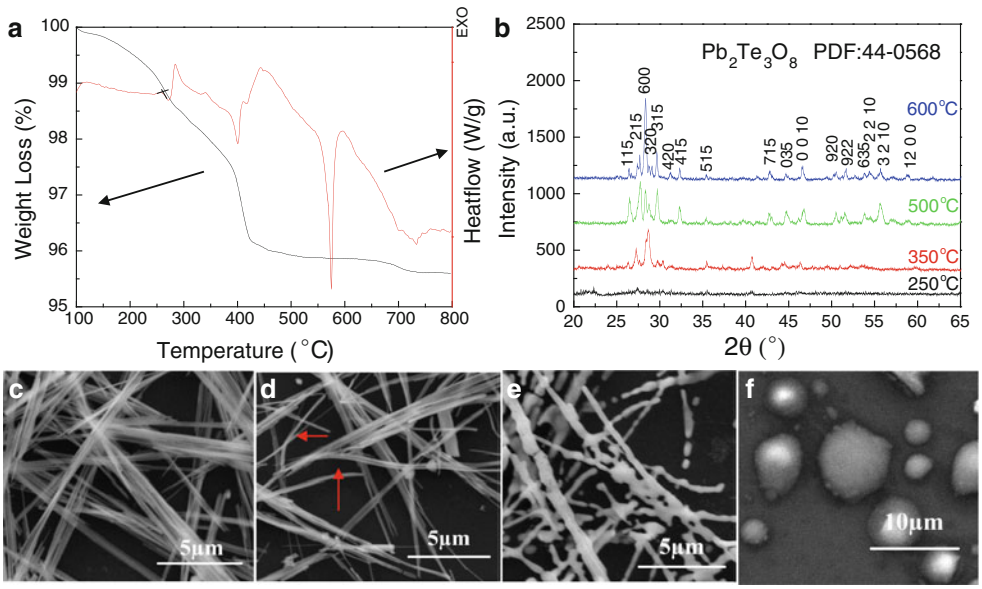

Fig. 3 **a** TGA and DSC curves of lead tellurite sample, **b** XRD spectra and **c–f** SEM images of lead tellurite nanobelts annealing in N_2 atmosphere at 250, 350, 500, and 600°C, respectively

Optical Properties

The energy gap (E_g) value of lead tellurite nanobelts can be calculated from the wavelength of the ultraviolet cutoff of the optical diffuse reflectance spectrum. The spectrum of the lead nanobelts is given in Fig. 4a. Because the size of individual nanobelt is much less than the thickness of the sample, which is prepared by casting the dispersed lead tellurite nanobelts in ethanol solution on a dielectric substrate, an ideal diffuse reflectance with constant scattering coefficient could be expected. The Kubelka–Munk function, which is the ratio between the absorption and scattering factor, is used for the absorbance plotting (Fig. 4a) and shows a clear optical gap at about 3.72 and 4.12 eV. It is indicated that the lead tellurite nanobelts are indirect band gap semiconductor, and the enlarged optical band gap is obvious relative to the corresponding bulky glasses (ca. 2.82–2.95 eV) [22, 31]. Figure 4b gives the FT-IR spectrum of the lead tellurite. The two absorption bands at 724 and 629 cm^{-1} in Fig. 4b are owing to equatorial asymmetric vibrations of Te–O_{eq} bonds and axial symmetric vibrations of Te–O_{ax} bonds [32], respectively. Due to the incorporation of Pb^{2+} ions as network modifiers to have formed new nonbridging oxygens in Te–$O^{-}\cdots Pb^{2+}\cdots{}^{-}$O–Te linkages, both bands shift toward lower frequency and they appear broader than those of crystalline TeO_2 [28]. Two nearby peaks at 1,350 and 1,380 cm^{-1} are attributed to vibrations of bridging oxygen between the [TeO_3] and [TeO_4] groups. The broad absorption band around 3,427 cm^{-1} is caused by the presence of OH^{-} groups in the glass matrix, which corresponds to the fundamental vibration of OH^{-} groups [33]. The weak absorption of OH^{-} groups shows a small quantity of Te–OH in this glass network.

The optical properties of as-prepared lead tellurite nanobelts were investigated via fluorescence imaging and PL spectrum. Figure 5a, b shows bright-field and fluorescence image of the lead tellurite nanobelts under UV light excitation at room-temperature, respectively. The nanobelts can be clearly distinguished in the fluorescence image corresponding to the bright-field image in Fig. 5b, indicating their potential use in biological labeling. Detailed room and low-temperature PL properties of the nanobelts are given under the HeCd laser irradiation, as are shown in Fig. 5c. PL emission presents a broad peak centered at 481 nm under the excitation of 325 nm at room-temperature. With decrease in temperature, the blue luminescence peak becomes stronger except at 30 K. Below the temperature of 100 K, The intrinsic emission peak at 394 nm begins to appear. The photoluminescence properties of the lead tellurite nanobelts are attributed to the Pb^{2+} dimer centers in tellurite networks [34, 35]. It is shown that Pb^{2+} ions tend to form various types of aggregate centers besides Pb^{2+} monomer, and optical bands in the blue (430 nm) are due to Pb^{2+} dimer centers [35]. It is reported that the blue-emitting peaks shift toward the long wavelength with the increase in Pb^{2+} content in CaS:Pb films, and the peak shifts to around 480 nm at the Pb^{2+} content of 2.2 at% [34]. As the lead tellurite nanobelts have a large number of the blue-emitting luminescent centers (the Pb^{2+} dimmers), the blue-emitting band is shifted to 481 nm.

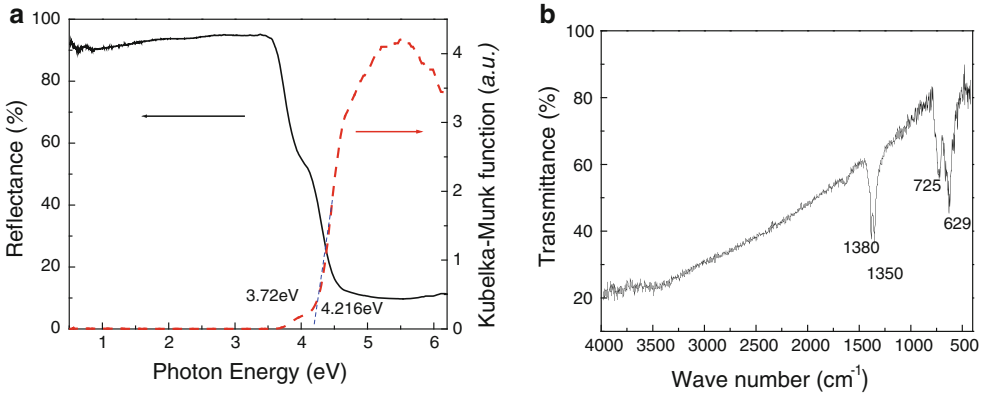

Fig. 4 **a** The optical diffuse reflectance spectrum and Kubelka–Munk function and **b** FTIR spectra of lead tellurite nanobelts

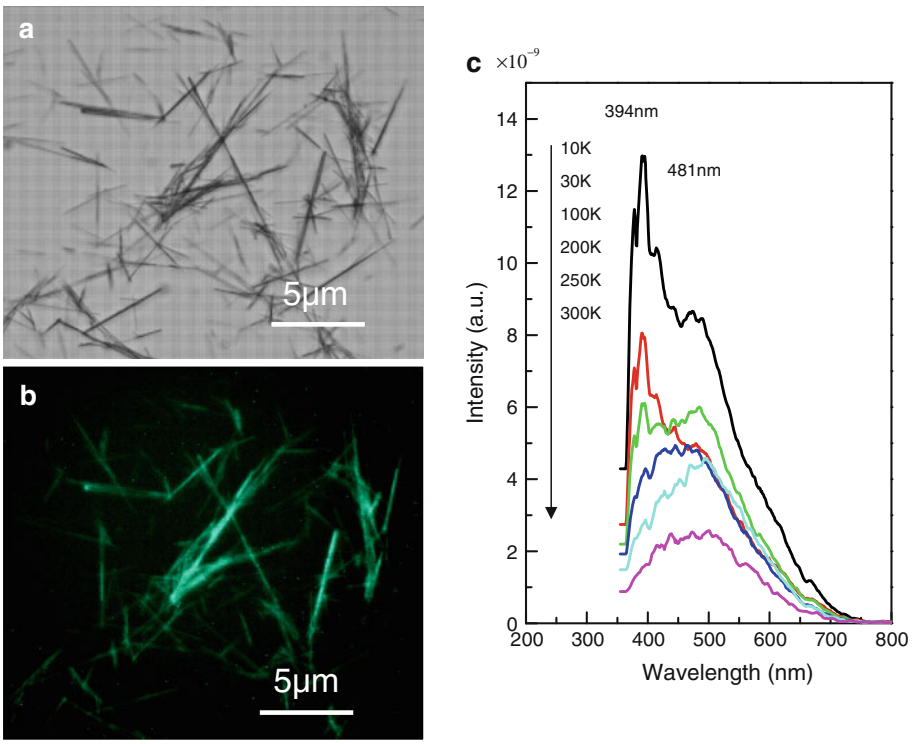

Fig. 5 **a** Bright-field and **b** fluorescence images of lead tellurite nanobelts under UV excitation, **c** room-temperature and low-temperature fluorescence spectra of nanobelts under 325 nm laser excitation

Conclusions

We have achieved the synthesis of lead tellurite nanobelts with lengths up to tens of microns and width of 200–300 nm in the composite molten salts at ambient atmosphere. It is for the first time that the tellurite glassy nanomaterials are synthesized. The method is simple, easy to scale-up, and with no use of organic dispersant or surface capping agent. The nanobelts have the stoichiometry of $Pb_2Te_3O_8$ and possess a typical grassy structure and temperature-dependent sate transition characteristics. However, thermal stability, crystallization, and melting temperature of the glassy nanobelts is lower than that of bulk lead tellurite glass. The lead tellurite nanobelts can emit blue light under UV radiation at room-temperature, and the emission intensity is enhanced at low-temperature. We believe that the lead tellurite nanobelts are promising for optical devices and biological labeling.

Acknowledgments This work has been funded by the NSFC (60976055, 50872070), NSFDYS: 50925205, the Science and Technology Research Project of Chongqing Municipal Education Commission of China (KJ080819), and Postgraduates' Science and Innovation Fund (200801CIA0080267), Innovative Training Project (S-09109) of the 3rd-211 Project, and sharing fund of large-scale equipment of Chongqing University.

References

1. R.A.F. El-Mallaway, *Tellurite Glasses Handbook: Properties and Data* (CRC, Boca Raton, 2002)
2. J.S. Wang, E.M. Vogel, E. Snitzer, Opt. Mater. **3**, 187 (1994)
3. K.S. Bindra, H.T. Bookey, A.K. Kar, B.S. Wherrett, X. Liu, A. Jha, Appl. Phys. Lett. **79**, 1939 (2001)
4. Y.Q. Li, Z.R. Sun, H.F. Kang, Y.Z. Yuan, Z.G. Wang, J. Rare Earths **25**, 412 (2007)
5. S. Kim, T. Yoko, S. Sakka, J. Am. Ceram. Soc. **76**, 865 (1993)
6. H. Nasu, O. Matsushita, K. Kamiya, H. Kobayashi, K. Kubodera, J. Non Cryst. Solids **124**, 275 (1990)
7. N. Jaba, H.B. Mansour, B. Champagnon, Opt. Mater. **31**, 1242 (2009)
8. R. Debnath, A. Ghosh, S. Balaji, Chem. Phys. Lett. **474**, 331 (2009)
9. Q.H. Nie, X.J. Li, S.X. Dai, T.F. Xu, Z. Jin, X.H. Zhang, J. Lumin. **128**, 135 (2008)
10. T.F. Xu, X. Shen, Q.H. Nie, Y. Gao, Opt. Mater. **28**, 241 (2006)
11. Z. Jin, Q.H. Nie, T.F. Xu, S.X. Dai, X. Shen, X.H. Zhang, Mater. Chem. Phys. **104**, 62 (2007)
12. A. Nayak, P. Kundu, R. Debnath, J. Non Cryst. Solids **353**, 1414 (2007)
13. A. Mori, Y. Ohishi, S. Sudo, Electron. Lett. **33**, 863 (1997)
14. A. Lin, A. Zhang, E.J. Bushong, J. Toulouse, Opt. Express. **17**, 16716 (2009)
15. A.I. Hochbaum, R.K. Chen, R.D. Delgado, W.J. Liang, E.C. Garnett, M. Najarian, A. Majumdar, P.D. Yang, Nature **451**, 163-U5 (2008)
16. P.D. Kanungo, R. Kögler, P. Werner, U. Gösele, W. Skorupa, Nanoscale Res. Lett. **5**, 243 (2010)
17. Z.H. Wang, J. Wei, P. Morse, J.G. Dash, O.E. Vilches, D.H. Cobden, Science **327**, 552 (2010)
18. K. Chu, H. Guo, C. Jia, F.G. Yin, X. Zhang, X. Liang, H. Chen, Nanoscale Res. Lett. doi:10.1007/s11671-010-9577-2
19. P.X. Gao, Y. Ding, W.J. Mai, W.L. Hughes, C. Lao, Z.L. Wang, Science **309**, 1700 (2005)
20. D.E. Zhang, X.D. Pan, H. Zhu, S.Z. Li, G.Y. Xu, X.B. Zhang, A.L. Ying, Z.W. Tong, Nanoscale Res. Lett. **3**, 284 (2008)
21. T. Komatsu, H.G. Kim, H.J. Mohri, Mater. Sci. Lett. **15**, 2026 (1996)
22. M. Vithal, P. Nachimuthu, T. Banu, R. Jagannathan, J. Appl. Phys. **81**, 7922 (1997)
23. R.F. Cuevas, A.M. de Paula, C.L. Cesar, L.C. Barbosa, O.L. Alves, Quim. Nova **21**, 361 (1998)
24. R.M. Reddy, B.S. Raju, N. Veeraiah, Bull. Mater. Sci. **24**, 63 (2001)
25. P. Subbalakshmi, P.S. Sastry, N. Veeraiah, Phys. Chem. Glasses **42**, 307 (2001)
26. L.R. Pederson, J. Electron Spectrosc. Relat. Phenom. **28**, 203 (1982)
27. W.E. Swartz Jr., K.J. Wynne, D.M. Hercules, Anal. Chem. **43**, 1884 (1971)
28. M.D. Munoz-Martín, M.A. Villegas, J. Gonzalo, J.M. Fernández-Navarro, J. Eur. Ceram. Soc. **29**, 2903 (2009)
29. M.D. O'Donnell, C.A. Miller, D. Furniss, V.K. Tikhomirov, A.B. Seddon, J. Non Cryst. Solids **331**, 48 (2003)
30. R. El-Mallawany, R. J. Mater. Res. **18**, 402 (2003)
31. V.K. Rai, L.de S. Menezes, C.B. de Dearaújo, Appl. Phys. A **91**, 441 (2008)
32. P. Armand, P. Charton, Phys. Chem. Glasses **43**, 291 (2002)
33. J. Pedlíková, D. Ležal, P. Kostka, J. Zavadil, J. Non-Cryst, Solids **326, 327**, 42 (2003)
34. Y.S. Kim, S.J. Yun, J. Phys. Condens. Matter **16**, 569 (2004)
35. C.B. de Araújo, L.R.P. Kassab, R.A. Kobayashi, L.P. Naranjo, P.A.S. Cruz, J. Appl. Phys. **99**, 123522 (2006)